J. Fluid Mech. (1999), *vol.* 387, *pp.* 129–150. Printed in the United Kingdom

Detachment phenomena in low Reynolds number flows through sinusoidally constricted tubes

By G. LENEWEIT† AND D. AUERBACH

Max-Planck-Institut für Strömungsforschung, Bunsenstr. 10, D-37073 Göttingen

(Received 9 September 1995 and in revised form 30 November 1998)

We examine the nature of detachment experimentally and numerically in steady axisymmetric flows through sinusoidally constricted tubes with Re varying from 10^{-4} to 10^2. Various regions can be distinguished, including flow detachment at the lowest Re used. Further, the transition in the pressure drop from a linear Poiseuille-like behaviour to a nonlinear pressure-drop–velocity relationship is not generally related to the appearance of detachment regions but rather to their form and to the nature of their growth. For the geometries considered here, the relationship between the start of nonlinearity in the pressure drop and incipient detachment depends on whether detachment is symmetric (detachment point at the bottom of a trough): for flow geometries with symmetric incipient detachment kinematic changes occur at Re lower than or the same as that at which dynamic changes can be detected, whereas for those with asymmetric incipient detachment they occur at higher Re. We look at various possible criteria for determining the transition from the viscous to the inertial range. Finally, we discuss the effect of elongational terms in the energy dissipation on flow through periodically constricted tubes and compare this flow with flow through porous media.

1. Introduction

The conditions under which flow detaches and the dynamic consequences are one of the fundamental areas of fluid mechanics research, occurring in many fields of flow science and technology. We will be concerned with laminar flows through periodically constricted tubes from the inertial down to the creeping flow regime. This geometry has become a popular model of flows in such varied fields as stenosed arteries and blood oxygenators, in flow-off problems as well as in leaching and filtration in natural and artificial situations, the latter involving the flow through porous media. For creeping flow (nominally $Re < 1$) it was long a belief, perhaps fostered by the Hele-Shaw/potential analogy, that when inertial effects become negligible the flow will remain attached (see also e.g. the remarks by Jeffrey & Sherwood 1980). This belief was perhaps nurtured by the experimental observation in diverging channels that the adverse pressure gradient associated with inertial forces is a prerequisite for flow detachment. Moffatt (1964) was the first to prove viscous detachment to be a widespread effect by analytically studying Stokes flow in a wedge-shaped cavity flow. Other authors subsequently investigated various configurations, such as two in-line

† Present address: Carl Gustav Carus-Institut, Am Eichhof, 75223 Niefern-Öschelbronn, Germany.

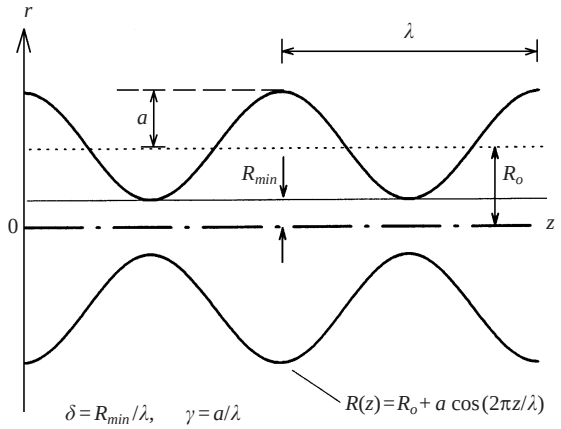

FIGURE 1. Sketch of the geometry with nomenclature.

spheres (Davis *et al.* 1976), a cylinder in the neighbourhood of a wall (Davis & O'Neill 1977) or two cylinders arranged perpendicular to the main flow (Dorrepaal & O'Neill 1979), all of which yielded Stokes flow detachment (for $Re \rightarrow 0$). The first experimental demonstration of creeping flow detachment was made by Collins (1979) for a spherical cap and by Taneda (1979) for several other geometries. A combined analytical and experimental study of steady creeping cylindrical Couette flow past a wavy-walled inner cylinder was done by Munson, Rangwalla & Mann (1985), where the conditions for flow detachment were explored in their dependence on the wavelength and amplitude of the wall form, as well as on the mean channel width. However, most analytical approaches only focused on kinematic effects, and were often only qualitative due to the approximations applied. Moreover, the theoretical and experimental studies mentioned above dealt with creeping flow, allowing no variation in the Reynolds number. Thus, despite theoretical and experimental efforts in the prediction of geometrical configurations containing regions of flow detachment, a deeper understanding of the mechanism of detachment in creeping flows and its relation and relevance to detachment at low and moderate *Re* is still lacking.

For flow in periodically constricted tubes as shown in figure 1 – (in our case, one generated by the surface of revolution of a cosine function about the axis of symmetry) – Chow & Soda (1972) did an asymptotic analysis for large wavelengths, which yielded detachment down to creeping-flow Reynolds numbers. Lahbabi & Chang (1986) investigated the flow field numerically and Deiber & Schowalter (1979), Ralph (1987) and Deiber *et al.* (1992) performed experimental and numerical studies. Nishimura, Yoshiji & Kawamura (1983), Sobey (1980) and Stephanoff, Sobey & Bellhouse (1980) did numerical and experimental work on the analogous channel geometry, the latter two on time-dependent pulsatile flows, and Guzman & Amon (1996) investigated their chaotic behaviour. All publications on periodically constricted tubes or channels cited above solved the complete Navier–Stokes equations (either steady or unsteady) and dealt mainly with the influence of the nonlinear terms and the transition to turbulence. Pilitsis & Beris (1991) included non-Newtonian effects for tube flow. The question of creeping-flow detachment, however, received no more than a glancing interest from the above authors. On the other hand, Fedkiw & Newman (1977, 1987), Neira & Payatakes (1979) and Tilton & Payatakes (1984) solved the Stokes equations numerically for a sinusoidally constricted tube to investigate friction effects in porous

media. Hemmat & Borhan (1995) did the same, and they paid some attention to flow detachment in the creeping regime.

When viewing the present state of research, one can name three fields in which the preceding work came to no or only contradicting results. Firstly, there has been no experimental verification of the predicted conditions for Stokes flow detachment so far, despite large discrepancies between the different authors for stronger tube constrictions (see Hemmat & Borhan 1995). Secondly, no work has been undertaken to compare the conditions for detachment in creeping (Stokes) flow with those of low Reynolds number flow or flow at moderate *Re*. Thirdly, different authors have made contradictory statements about the relationship between incipient flow detachment and the departure from a linear dependence of the pressure drop on the mean flow rate. Two authors proposed a general coincidence of these two events based on their experimental and numerical findings (Deiber & Schowalter 1979 and Ralph 1987), whereas Lahbabi & Chang (1986) showed a difference of one order of magnitude in *Re* in a numerical study. Each of the above papers dealt with a single specific geometry. Therefore we shall concentrate our work on three topics: (i) Conditions for the existence of creeping flow detachment; (ii) changes in the detachment behaviour with *Re* growing to low or moderate values, and (iii) possible relationships to dynamic changes. The ultimate aim of the study is to give an improved basis for the understanding of the detachment mechanisms in the different flow ranges.

The last topic we will broach is the relationship between the above tube flow and the flow through porous media. Since its introduction by Petersen (1954) constricted tube flow has become a popular model for the flow through porous media. The linear Darcy–Kozeny law is often used for low Reynolds number flow, even though criticism of its use here is almost as old as the law itself (see for example Forchheimer 1901) and a perennial topic (Firdaouss, Guermond & Le Quéré 1997). This model for porous flow is fraught with problems because of, amongst others, nonlinear terms in the pressure–velocity correlation that influence the flow, even at $Re = O(1)$, which are still the subject of intensive research (see for example Rasoloarijaona & Auriault 1994; Kececioglu & Jiang 1994; Andrade *et al.* 1995). A second problem concerns the coefficient of the linear term in the pressure–velocity correlation, which is higher than the theoretical approximations by a factor 2 to 3 (see e.g. Bird, Stewart & Lightfoot 1960, p. 196 for a theoretical estimation and Ergun 1952 for experimental results). Durst, Haas & Interthal (1987) suggested that the discrepancy between theory and experiment was due to the oversimplification of the flow field by modelling it as an array of straight capillary tubes whose diameter is determined by means of the hydraulic radius concept. They speculated that the neglected elongational strain terms in the determination of the energy dissipation would be responsible for the difference between theory and experiment. Unlike the flow geometry of a randomly packed bed of spheres that they consider, our flow geometry admits a simple estimation of the ratio of elongational strain to shear terms in the limit $Re \to 0$.

2. Experimental set-up and numerical methods

2.1. *Experimental set-up*

Experiments were performed with six different tube geometries. From the three governing dimensional parameters, the minimum radius $R_{min} = R_o - a$, the wavelength λ and the amplitude a (see figure 1 for definitions), two dimensionless parameters

λ (mm)	γ	δ	δ_{Ro}	Total number of segments
53.33	0.15	0.17	0.32	9
38.46	0.15	0.35	0.5	12
21.74	0.15	0.85	1	22
47.05	0.21	0.11	0.32	10
35.29	0.21	0.29	0.5	14
20.62	0.21	0.79	1	24

TABLE 1. Geometrical parameters of the periodically constricted tubes used in the experiments.

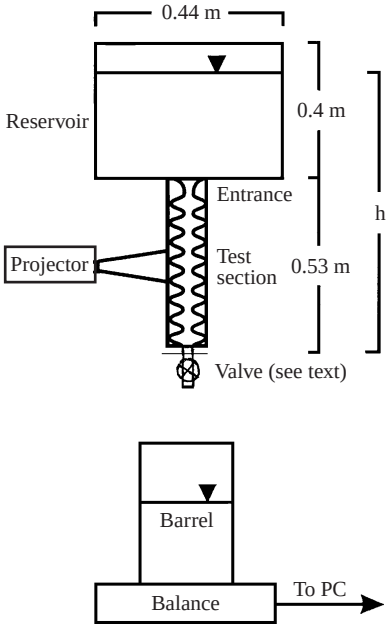

FIGURE 2. Experimental set-up.

$\gamma = a/\lambda$ and $\delta = R_{min}/\lambda$, can be formed. For an easier comparison with other results, we also show the parameter δ defined with the mean radius: $\delta_{Ro} = \delta + \gamma$. For fixed λ, reducing δ means narrowing tubes, reducing γ means flattening the wave. Two different values of γ and three different values of δ_{Ro} were investigated. The values of λ, γ, δ, δ_{Ro} and the total number of segments for each geometry used in the experiments are given in table 1.

The tubes were made by CNC milling segments of Plexiglas of length λ and polishing them to achieve transparent surfaces. The segments varied by a maximum of 25 μm from an ideal cosine of revolution. All segments for a particular parameter combination were slid into a glass tube of length $l = 0.53$ m and diameter 60 ± 0.02 mm (see sketch of the apparatus in figure 2). This allowed an easy change of parameters. The segments had an outer diameter of 59.7 mm, so that the alignment between segments was out by no more than 0.3 mm. Owing to this set-up, all constricted tubes

had a maximum inner diameter of 50 mm. Even though the slit between constriction segments and the glass tube was filled with silicon oil, the glass tube itself being submerged in silicon oil enclosed by a box of Plexiglas with parallel walls and a square cross-section (all the materials employed: silicon oil, Duran glass and Plexiglas have very similar refractive indices $n = 1.404;\ 1.473;\ 1.490$ respectively), optical distortion of the flow patterns inside the constricted tube could not be suppressed entirely. Therefore, a millimetre grid that served as a reference was introduced into the mid-plane (the longitudinal section containing the tube's axis) of each constricted tube and photographs were taken in the direction perpendicular to the grid plane of the tubes when filled. These reference photographs showed distortion to be negligible for the constricted tubes with $\delta \leqslant 0.17$. For all other tubes the evaluation of the experimentally obtained detachment and reattachment points had to be done using the reference grid photos to eliminate distortion.

The reservoir and the test section were filled with silicon oil and left standing for up to twelve hours to allow air bubbles to surface. Each run began by opening a valve – either of a stopcock or of a flange-type (see justification presently) – at the bottom of the tube. Oil flowed out as a free jet into a barrel standing on a balance. The weight was recorded via a PC every second, and from this mass flux both the volume flux Q and the pressure head h were calculated as the reservoir drained. The oil left the reservoir via a short constrictor some 50 mm long and both entered and left the test section at its largest constriction. In order to allow a continuous variation of the head as well as to avoid frictional heating, no pump was used, the reservoir simply being refilled by hand. The room temperature changed by less than 0.2 °C during the longest runs of 2 hours. The kinematic viscosity ν of the different silicon oils (ν varied from 100 to 60 000 $\mathrm{mm^2\,s^{-1}}$) was measured by means of several capillary viscometers (to cover the entire range) stabilized to ± 0.1 °C in a temperature-controlled bath. The overall accuracy in the determination of the oil's viscosity was around $\pm 2\%$.

For kinematic measurements tracer particles of 28 to 50 μm in diameter were mixed into the fluid and a 1 mm thick light sheet was projected through the axis of the tube. Long-exposure photographs yielded pathlines of the two-dimensional steady flow field (see figures 3 and 4). The Reynolds number

$$Re = 2R_{min}\,\bar{u}/\nu \quad \text{with} \quad \bar{u} = Q/(\pi R_{min}^2) \tag{2.1}$$

was varied by increasing or decreasing Q with the stopcock-type valve mentioned above.

For pressure drop measurements Re could not be varied by means of a stopcock since these were made by reading off the pressure head, and would thus have been falsified by throttling. Re was therefore varied by changing the viscosity in ten steps by mixing oils of different viscosities. The stopcock was replaced by a flange (see figure 2). The pressure loss due to the flow into the entrance was approximated by assuming a Poiseuille relation to hold (with the volume flux Q and a suitable mean radius). A second correction was applied to account for the dynamic pressure loss at higher Re by subtracting the dynamic pressure $\frac{1}{2}\rho\bar{u}^2$ from the static pressure loss. Thus, the effective pressure loss over the full length of the periodically constricted tube reads as follows:

$$\Delta p_{eff} = \rho g h - \Delta p_{entrance} - \tfrac{1}{2}\rho\bar{u}^2.$$

There is a further pressure loss due to viscosity slowing the flow along the floor of the reservoir and along the more or less dirty free surface. These only become important for low heads, which we thus avoided. We defined a modified Fanning

friction factor of the wavy walled tube as

$$f = \frac{\Delta p_{eff}}{\rho \bar{u}^2} \frac{R_{min}}{n\lambda}, \tag{2.2}$$

n being the number of segments used. Strictly speaking the above draining flow is unsteady with a time scale of $\tau = (h - l)\mu l R_{res}^2/(\rho g h R_{min}^4)$ (using Hagen–Poiseuille's law for the depletion of the reservoir with R_{res} the reservoir radius). The mean tube velocity $\bar{u}$ is proportional to $\rho g h R_{min}^2/(\mu l)$ and thus the Strouhal number $Sr = R_{min}/(\bar{u}\tau) = R_{min}/((h - l)R_{res}^2)$, which is of the order of 10^{-3} for the worst cases. We may thus regard the flow as being steady. For more details on the measurements themselves see Leneweit (1995).

2.2. *Numerical calculations*

Numerical solutions of the Navier–Stokes equations for incompressible steady Newtonian flow were obtained by means of a finite volume method. Its main features are described in Perić (1985) and Perić, Kessler & Scheuerer (1988). The equations of motion for two-dimensional, axisymmetric flow are solved in the primitive variable formulation (velocity $\boldsymbol{u}$ and pressure p). A non-staggered variable arrangement is used and a stabilization term added to prevent the decoupling of velocity and pressure. Non-orthogonal grids are generated that allow an easy variation of the geometry.

Discretization of the convective terms could be performed optionally up to first, second or third order. We chose second-order central differences for our calculations. For the coupling of pressure and velocity a SIMPLE algorithm after Patankar & Spalding (1972) was implemented and an incomplete lower-upper decomposition after Stone (1968) was used for solving the algebraic equations. The programme makes use of a multi-grid scheme to accelerate convergence and our calculations were performed on four grid levels, the finest grid consisting of 80×160 volume elements.

3. Results

3.1. *Kinematic results*

Figure 3 shows streamlines of the entire flow field, illustrating asymmetric detachment due to inertia for $Re = 17$, $\delta = 0.11$ and $\gamma = 0.21$. In contrast figure 4 illustrates symmetric Stokes flow for $Re = 0.025$, $\delta = 0.79$ and $\gamma = 0.21$. In the following we shall discuss the form and extent of the detachment region, characterized by the occurrence and position of the detachment and reattachment points ('points' are really lines and lines are really surfaces). We then discuss the conditions for incipient detachment (general considerations and the effect of changing γ) and the effects of increasing Re, changing the boundary conditions, the velocity profile and the scaling radius.

3.1.1. *The form of the detachment region*

When the flow was detached this region took the form of a ring-shaped recirculation zone. The two main differences between figures 3 and 4 are the extent of the recirculation zone and the upstream/downstream symmetry. Although the form of the detachment streamline (whether it is convex or concave, inflection points, etc.) would certainly need a more detailed quantitative investigation we will first give a short qualitative survey, followed by a detailed description of the detachment and reattachment points in the next section. The variation of the upstream/downstream symmetry with growing Re for the four extremes of small and large values of δ

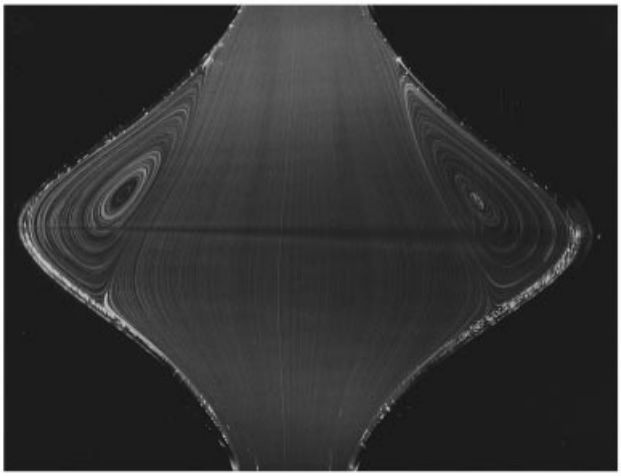

FIGURE 3. Streamlines of the entire flow field for one wavelength (flow from top to bottom) illustrating asymmetric detachment due to inertia. $Re = 17$; $\delta = 0.11$; $\gamma = 0.21$. Exposure time: 10 s.

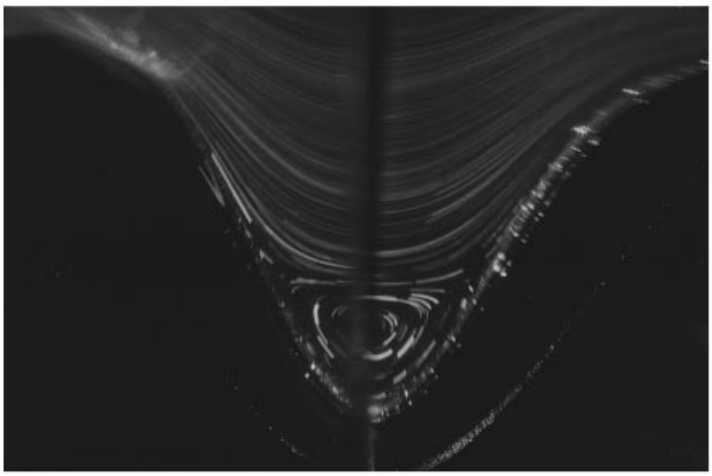

FIGURE 4. Streamlines of the trough region in the creeping regime illustrating symmetric detachment (flow from left to right). $Re = 0.025$; $\delta = 0.79$; $\gamma = 0.21$. Exposure time: 600 s.

and γ is summarized in figure 5. Here we see that small δ yields attached creeping flows (i) whereas a symmetrically detached creeping flow is achieved for large δ (ii). Symmetrically detached flow beginning at a low Reynolds number only takes place for small δ and large γ (iii). For the fourth parameter combination with small δ and γ, initial flow detachment at low Re is asymmetric and in all other cases the creeping flow detachment zones become asymmetric in the low Re range (iv). In all these cases the downstream streamline is depressed. It is interesting to note that for viscoelastic fluids it is the upstream end of the streamline which is depressed, even for creeping flow (Pilitsis & Beris 1991). All parameter combinations share the common feature that the detachment zones tend to symmetry, not only in the creeping-flow range but also in the high-Re limit of laminar flow (apart from a short asymmetric 'tail' remaining near the reattachment point). A further increase in Re leads to the transition to turbulence

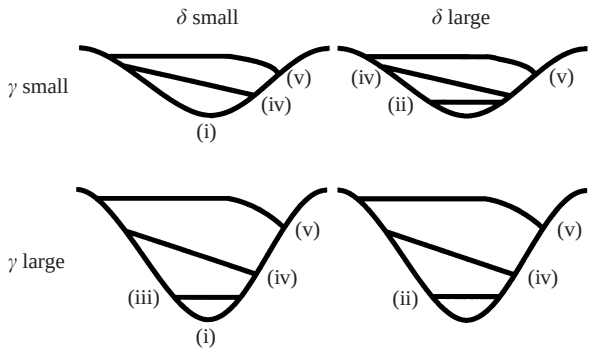

FIGURE 5. Variation of symmetry with growing Re for small and large values of δ and γ in tabular form: (i) creeping flow attached, (ii) creeping flow symmetrically detached, (iii) low Re symmetric detachment, (iv) low Re asymmetric detachment, (v) laminar high Re limit.

with the detachment zones becoming oscillatory (Nishimura *et al.* 1984; Lahbabi & Chang 1986; Guzman & Amon 1996). In the following we shall characterize the extent of the detachment region by the detachment and reattachment points alone.

3.1.2. *The extent of the detachment region*

We first report on the behaviour of the detachment zone for a fixed amplitude-to-wavelength ratio $\gamma = 0.21$ when Re is increased between 10^{-2} and 10^{2} as the dimensionless mean radius δ grows ($0.11 < \delta < 0.79$). Results of numerical calculations are included in figure 6. The larger the Reynolds number, the better the agreement between experiment and numerical simulation, a strange result at first glance. This behaviour is most likely due to the difficulty in experimentally resolving the detachment zone when it is small and restricted to the bottom of the cavity. The fact that there is no experimental detachment zone for $\delta = 0.11$ and $Re < 5.8$ ought not be seen as a contradiction to simulations, since the detachment zone must be large enough for a closed pathline of at least one tracer particle to be followed. We thus could not resolve the flow in more detail. The most apparent feature in figure 6 is that the detachment zones grow with increasing Re for all fixed δ and γ. The same holds for increasing γ for fixed δ and Re (cf. figures 6 and 7). This cannot be said with the same generality on changing δ: for $Re < 10$ the detachment zone grows with growing δ but for $Re > 20$ the opposite holds. For $\delta \geqslant 0.29$ the width of the detachment zone remains constant in the creeping-flow range, whereas for $\delta = 0.11$ the detachment zone diminishes with decreasing Re and finally vanishes at $Re = 1.5$. The detachment zones for $\delta \geqslant 0.29$ remain symmetric with respect to the $z = 0$ plane and constant in size up to some limiting $Re = Re_{kl}$ (kinematic limit), where two things occur simultaneously: symmetry is lost and there is an abrupt increase in the width of the detachment zone ($Re_{kl} \approx 3.4$ for $\delta = 0.29$ and $Re_{kl} \approx 11.4$ for $\delta = 0.79$). The seemingly parallel and vertical lines indicate that for these δ-values detachment takes place in the creeping-flow limit, for they showed no sign of converging, even for the lowest Re considered.

The results in figure 7 with flatter wavy walls ($\gamma = 0.15$) are essentially the same as those in figure 6. Here none of the curves shows Stokes flow detachment and the Reynolds number of incipient detachment Re_{det} decreases with increasing δ as it did in figure 6. The curve for $\delta = 0.17$ indicates a parabolic increase in size with growing Re (no inflection points, see figure 7) and its detachment zone, unsymmetrical at low

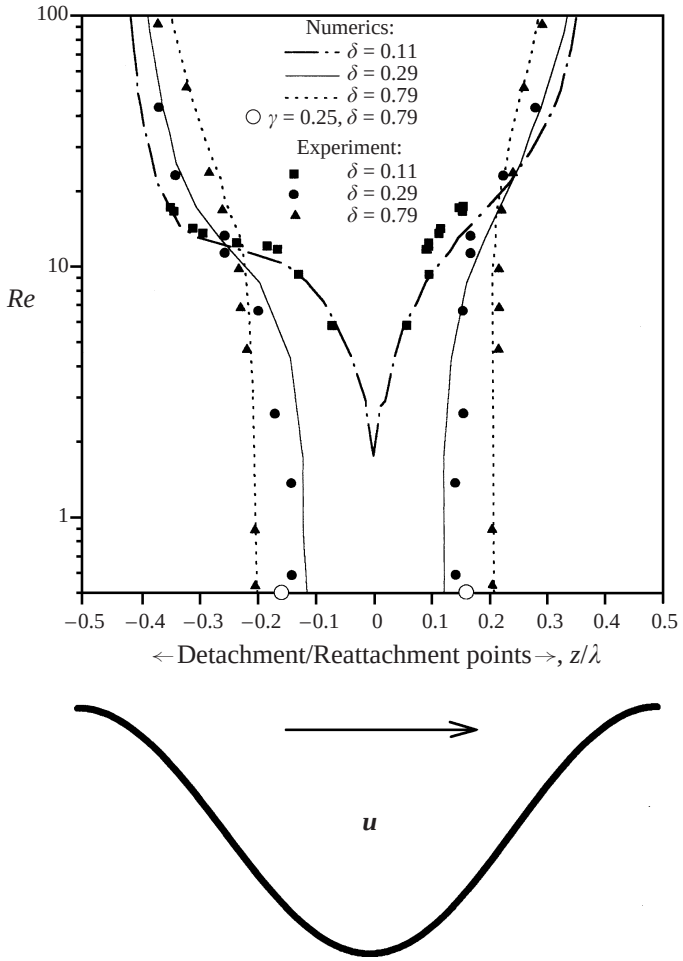

FIGURE 6. The dependence of the detachment and reattachment points on Re with $\gamma = 0.21$. The wave form (same scale as the abscissa) is included below to give an impression of the real geometry. The hollow circles for $\gamma = 0.5$ and $\delta = 0.25$ are from Pilitsis & Beris (1991).

Re, becomes increasingly symmetrical at higher Re. For $\delta = 0.35$, Re_{det} is decreased only slightly. Here the point of incipient detachment is in the trough (thus symmetric). The detachment region moves upstream and becomes asymmetric the moment Re increases. For $\delta = 0.85$ Re_{det} is decreased drastically, the detachment zone is symmetric up to $Re \leqslant 20$ and the two branches of the curve have inflection points like the curves in figure 6. The experimentally determined detachment zones must exceed a minimum size to become recognizable, so this may explain why we could not experimentally resolve incipient detachment any better. But since there is good agreement between experiment and numerics as soon as a finite detachment zone could be observed in the experiments, this gives credence to the numerically obtained v-shapes of the curves in both figures 6 and 7.

For completeness we have included Pilitsis & Beris' (1991) results in figure 6. The detachment region for $\gamma = 0.25$ and $\delta = 0.25$ is slightly larger than that for $\gamma = 0.21$ and $\delta = 0.29$. These additional results confirm the trend, that increasing γ increases the detachment zones at constant Re and δ, as can be observed comparing figures 6 and 7.

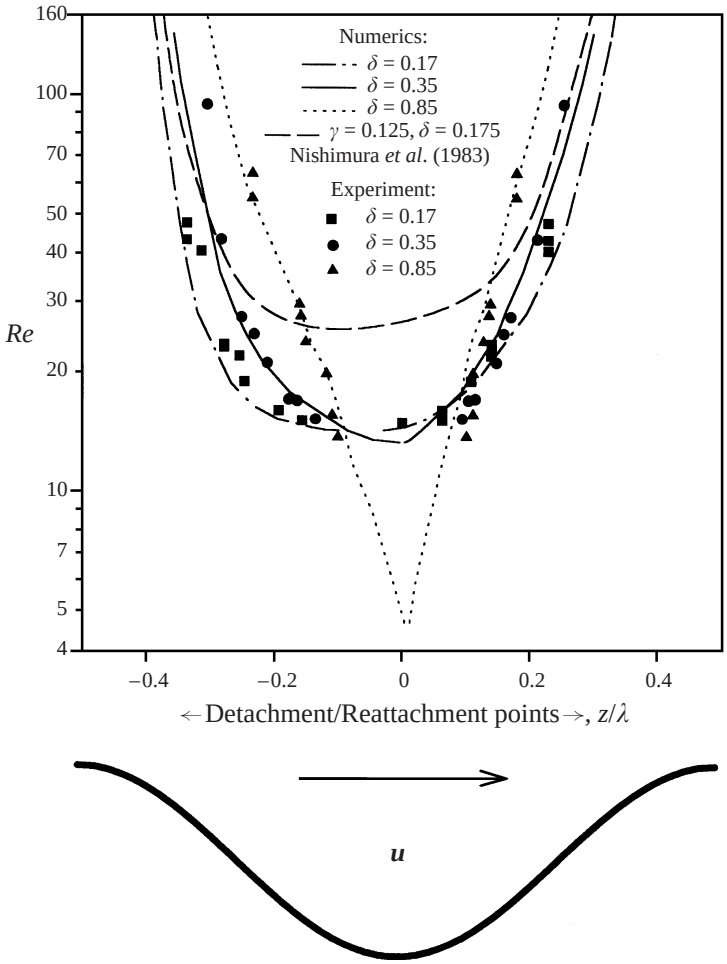

FIGURE 7. The dependence of the detachment and reattachment points on Re with $\gamma = 0.15$. The long dashed line is from Nishimura *et al.* (1983).

3.1.3. *Incipient detachment: symmetry*

Figure 7 ($\gamma = 0.15$) yields three Reynolds numbers at which detachment is just beginning. To get a better insight in the effect on Re_{det} when δ is varied (for $\gamma = 0.15$), the value of Re_{det} was iterated numerically for five further values of δ, the results of which are shown in figure 8. The solid curve represents Re_{det} (left ordinate) and the dashed curve indicates the location of incipient detachment (right ordinate). A boundary between symmetric and asymmetric detachment was made at the point $\delta \approx 0.35$. The value $\delta = 0$ corresponds to complete blockage of the tube, so that we considered values of $\delta \geqslant 0.1$. The solid curve divides the graph into two regions: for $Re - \delta$ combinations below the curve no detachment takes place; elsewhere we find detachment. The Re_{det} curve initially decreases with δ with a positive curvature down to an inflection point at $\delta \approx 0.35$ and then decreases with negative curvature until finally Stokes flow detachment is reached for $\delta \geqslant 0.94$. For $\delta \leqslant 0.35$ asymmetric detachment takes place, whereas incipient detachment for $\delta \geqslant 0.35$ is symmetric. In the region of symmetric detachment we can further distinguish between geometries where the flow has to reach a certain finite Reynolds number to cause flow detachment

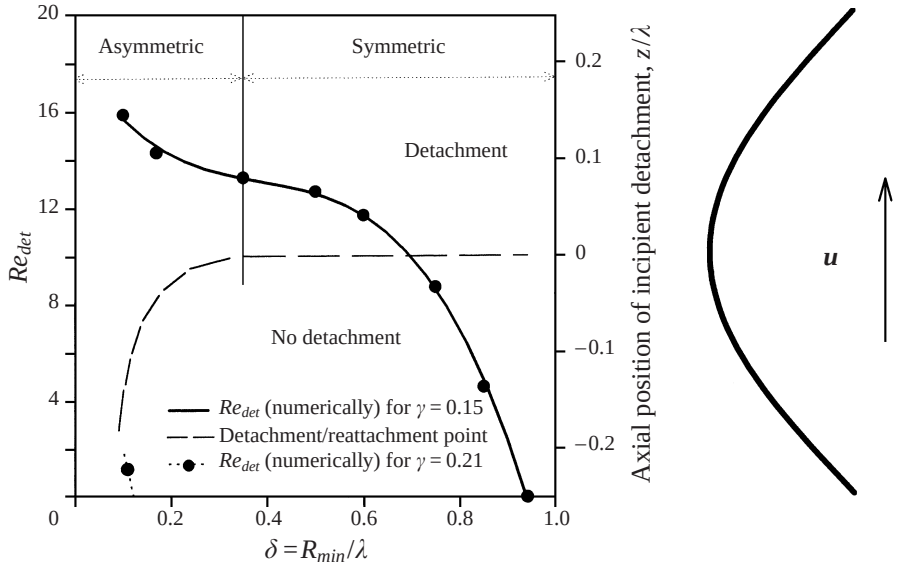

FIGURE 8. Numerical calculation of the Reynolds number at the beginning of detachment Re_{det} and axial position of incipient detachment versus δ with $\gamma = 0.15$ for all tube constrictions. The extent of the detachment zone is only one volume element at Re_{det}, therefore the detachment zone is traced with only one (dashed) line for $\delta \leqslant 0.94$. Symmetric bifurcation (not shown) occurs for $\delta \geqslant 0.94$. The point (with a short line) in the left bottom corner is for $\gamma = 0.21$.

(inertia not negligible), and those geometries that detach for all *Re* ($\delta \geqslant 0.94$ for figure 8). The latter case is referred to as creeping-flow detachment and the former as transitional detachment ($0.35 \leqslant \delta \leqslant 0.94$ for figure 8), since it lies between the creeping and the more clearly inertial detachment behaviour.

3.1.4. *Incipient detachment: increasing Re*

It is particularly interesting to note that all curves in figures 6 and 7 which show symmetric incipient detachment at Re_{det} have inflection points in the growth of the detachment regions with growing *Re* (i.e. all curves in figure 6 and the curve with $\delta = 0.85$ in figure 7). The curve with $\delta = 0.35$, $\gamma = 0.15$ in figure 7 has an inflection point in the shift of the reattachment point with growing *Re*, but no inflection point for the detachment point. As can be seen in figure 8, this geometry divides the regions between asymmetric and symmetric incipient detachment: the growth of the detachment region of those geometries with symmetric incipient detachment changes from a more than logarithmic growth to a less than logarithmic growth at higher *Re* as is the case for the curve with asymmetric detachment behaviour at Re_{det}.

3.1.5. *Incipient detachment: changing* γ

Since the simulations were intended for comparison with experimental results only those parameter combinations (with the exception of figure 8) studied experimentally were also numerically investigated. It is however possible to make a few general statements about the effect of changing γ. Figure 6 with $\gamma = 0.21$ and $\delta = 0.11$ yields but a single point, shown in figure 8. The other two δ-values with the same γ have creeping-flow detachment, so that there are no further points for this curve. We include a line segement to indicate the path which the incipient detachment line could follow there: an increase in γ shifts the intersection point to lower values of δ. The

limit of $\gamma \to 0$ yields a smooth tube without creeping-flow detachment, from which one can conclude that for $\gamma < 0.15$ the region for creeping-flow detachment is shifted to $\delta > 0.94$. Moffatt (1964) found that Stokes flow at a sharp corner whose angle of inclination α exceeded 159° attached. Smoothing this corner will further suppress detachment, so that one might well expect the $Re_{det} - \delta$ behaviour to converge to a horizontal asymptote for sufficiently small but finite γ.

3.1.6. *Incipient detachment: changing boundary conditions, axisymmetric vs. plane*

As mentioned in the introduction Nishimura *et al.* (1983) considered the plane channel case numerically and experimentally. One of their findings pertinent to our study is the extent of detachment in the creeping-flow regime as shown by the long-dashed curve in figure 7. Their value of $\delta = 0.175$ is closest to our $\delta = 0.17$ curve. This curve has $\gamma = 0.15$, slightly higher than their $\gamma = 0.125$. Comparing these curves not only confirms the tendency for Re_{det} to decrease as γ grows, but also confirms that a marked asymmetry is present in both planar and axisymmetric cases. This indicates that the detachment behaviour of plane flow is even quantitatively comparable to that of axisymmetric flow if the velocity profiles (Poiseuille flow, see next section) are similar.

3.1.7. *Incipient detachment: changing the velocity profile, Poiseuille vs. Couette flow*

One of the main kinematic results for creeping flow (figures 6 and 8) was that as the tube wall approaches the axis (decreasing δ at constant γ and Re) the size of the detachment zone decreases and ultimately vanishes. How does this result compare with the work of other authors? Munson *et al.* (1985) analytically and experimentally investigated Stokes flow detachment in a cylindrical Couette flow with a stationary inner wavy cylinder and a rotating outer cylinder. They theoretically confirmed that as the number of waves increased, their cylindrical flow became equivalent to a plane creeping Couette flow over a wavy wall with sinusoidal wall variations. For this straight-wall approximation they found that, as the plane wall approached the wavy wall, detachment is promoted. Does this result not stand in direct contradiction to our findings just mentioned? Apart from our axisymmetry and their channel-like flow (which, from considerations above, seem to make little difference) the main distinction between the flows is that in the Couette flow the velocity on the plane wall is constant – the elongational strain rate $\partial u_z/\partial z$ vanishes there (when z denotes the direction of the moving wall), as dictated by their boundary conditions. Contrarily, our centreline axial velocity varies continuously, thus $\partial u_z/\partial z \approx 0$. In our case, due to continuity, there is mass transport to the tube walls in the expanding part of the tube, which, in its turn, tends to suppress detachment. If both results are correct, low-Re detachment is sensitive to a change in the flow drive (pressure driven or wall driven), a fact which will need to be more closely considered for future theoretical work on more general cavity forms.

3.1.8. *Incipient detachment: changing the scaling radius*

The fact that the point $\delta \approx 0.35$ delineates the border both between the sign of the curvature of the Re_{det}–δ curve and between incipient a/symmetry (figure 8) merits more attention. To what extent is this no more than an accident due to our choice for the definition of Re? For example, almost all previous authors chose the mean radius R_o. To examine this effect we set an arbitrary radius $R_a = R_o + ka$ (a is the

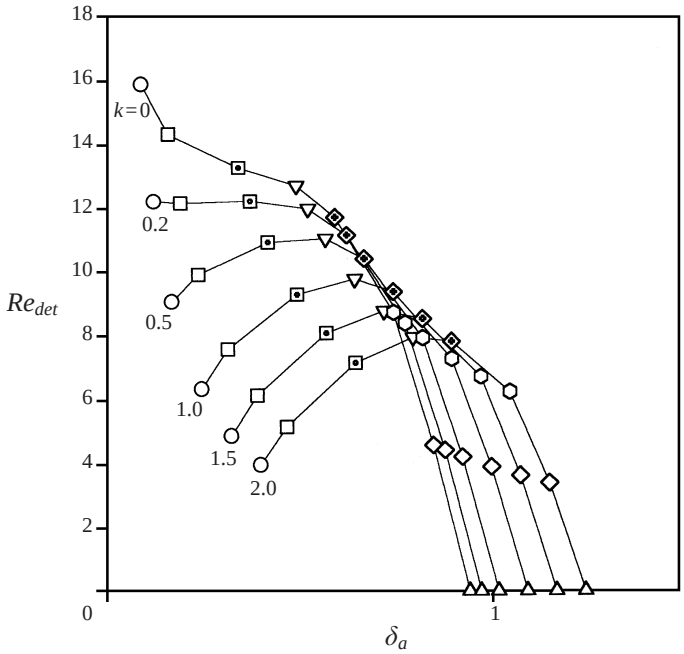

FIGURE 9. The effect of employing different scaling tube radii for Re_{det} vs. δ_a (equation (3.1)). The values of the parameter k are written to the left of each curve. The different symbols denote different geometries.

amplitude and $0 < k < 2$), which transforms

$$Re = \frac{2Q}{\pi R_{min} \nu}, \quad \delta = \frac{R_{min}}{\lambda}$$

to Re_a and δ_a according to

$$Re_a = \frac{R_{min}}{R_a} Re = \left(1 - \frac{k\gamma}{\delta_a}\right) Re, \quad \delta_a = \delta + k\gamma. \tag{3.1}$$

Figure 9 shows this representation for six choices of k. For $0 \leqslant k < 0.2$ the curve has an inflection point whereas for $0.2 < k \leqslant 2$ it has a maximum. The curve with $k \approx 0.2$ seems neutral. For an easier comparison the symbols on the curves were chosen such that physically identical geometries have the same symbol (e.g. open circles, open squares etc.), even though their δ_a-values differ according to (3.1). As can be seen the $\delta \approx 0.35$ point plays a special role only for the curve with $a = 0$.

3.2. *Dynamic results (pressure drop)*

The Stokes solution for a straight tube yields fRe=16. For wavy tubes table 2 contains the product fRe for different geometries and Re found by various authors as well as our results, which we used as a further test of the numerical method. Our experimental and numerical results show very good agreement with the numerical results of Lahbabi & Chang (1986), as well as with the other authors appearing in the table for the geometries which they considered. Figure 10 shows details of the pressure–velocity relationship in the form of an fRe versus Re plot for $\delta = 0.11$, $\gamma = 0.21$. Stokesian ($p \sim \bar{u}$) behaviour would appear as a horizontal line in this representation. In order to have a quantitative standard for the deviation from a

			fRe				
δ	γ	Re	This work	Lahbabi & Chang (1986)	Tilton & Payatakes (1984)	Fedkiw & Newman (1977)	Deiber *et al.* (1992)
0.35	0.15	0	8.20	8.28	7.97	6.15	8.15
0.1115	0.0477	0	6.36	6.35	6.40	6.57	6.36
0.1115	0.0477	17.1	6.50	6.52	—	—	6.61
0.1115	0.0477	72.8	7.61	7.63	—	—	7.74
0.1115	0.0477	188	8.78	8.83	—	—	—

TABLE 2. Comparison of different numerical predictions of the product fRe.

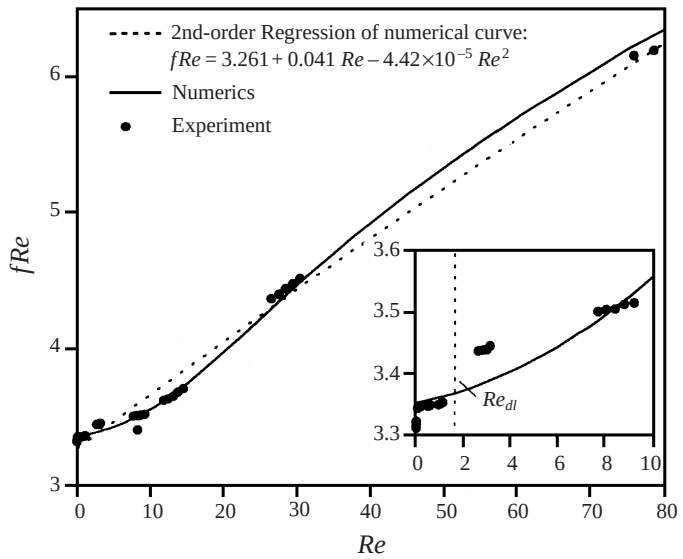

FIGURE 10. fRe versus Re with $\delta = 0.11$ and $\gamma = 0.21$, and an enlargement of the low Re-range.

linear behaviour, we define a limiting Reynolds number Re_{dl} ('dynamic limit' in the inset of figure 10) at which the value of fRe has become 0.5% larger than the value in the creeping-flow range ($Re = O(10^{-2})$). This definition is arbitrary since the fRe-curve remains gradual, but the 0.5% mark agrees quite well with the Reynolds number beyond which the slope becomes considerably steeper – see enlargement in figure 10. Using the 0.5% definition puts Re_{dl} at 1.75. Figure 10 also shows that there is a relatively large range $7.3 \leqslant Re \leqslant 58$, where fRe versus Re yields an effectively slanted straight line ($fRe \sim Re$), indicating that the pressure drop Δp through a periodically constricted tube can be reasonably well approximated by a second-degree polynomial in $\overline{u}$ ($\Delta p \sim \overline{u}^2$). For $Re > 58$ a gradual 'relinearization' takes place.

4. Discussion

How can we distinguish viscous from inertial behaviour? Is there a correspondence between kinematics and dynamics? How can we interpret the 'relinearization' at higher Re?

γ	δ	δ_{R_o}	Re_{det}	Re_{dl}	Re_{kl}
0.21	0.11	0.32	1.75	1.75	—
0.21	0.29	0.5	0	3.5	3.5
0.21	0.79	1	0	11.4	11.4
0.15	0.17	0.32	14.5	2.8	—
0.15	0.35	0.5	13.3	3.6	—
0.15	0.85	1	4.5	5.3	—

TABLE 3. Comparison of Re for the beginning of detachment: dynamic and kinematic limits.

4.1. *The transition from the viscous to the inertial region*

Four possible indices mark the transition from the viscous to the inertial regime: less-than-logarithmic growth of the detachment region; transition from symmetric to asymmetric incipient detachment; a change in the sign of the curvature of the $Re_{det} - \delta$ curves and a change in the pressure–velocity relationship. Numerical values are similar, sometimes even the same. For example, if we consider the coincidence of the threshold a/symmetry $Re - \delta$ value and the change in the sign of its curvature at $\delta \approx 0.35$, although the choice of the scaling radius is somewhat arbitrary, R_{min} is probably the most physically significant choice, determining the flow in the entrance region of each cavity. We shall now discuss the relationship between values for the dynamic and kinematic transition.

4.2. *Correspondence between kinematics and dynamics*

A general correspondence between a beginning nonlinearity in the pressure–velocity relation and the onset of flow detachment was suggested by Deiber & Schowalter (1979) and Ralph (1987), who indeed found this coincidence for their tube geometries at $Re \approx 75$ and 15 respectively (the Reynolds numbers are cited in the definitions of the respective authors). If, however, we examine table 3, which gives the results of our numerical calculations, such a coincidence can only be found for the geometries $\delta = 0.11$, $\gamma = 0.21$ and $\delta = 0.85$, $\gamma = 0.15$ with the Reynolds numbers $Re_{dl} \approx Re_{det} \approx 1.75$ and $Re_{dl} \approx 5.3$, $Re_{det} \approx 4.5$ respectively. For the other four geometries both effects occur separately. The two geometries, $\delta = 0.29$, $\gamma = 0.21$ and $\delta = 0.79$, $\gamma = 0.21$, show creeping-flow detachment ($Re_{det} = 0$) and therefore $Re_{dl} > Re_{det}$. For the remaining two geometries, $\delta = 0.17$, $\gamma = 0.15$ and $\delta = 0.35$, $\gamma = 0.15$, just the opposite holds: $Re_{dl} < Re_{det}$. We thus have three categories: Re_{det} larger than, Re_{det} approximately equal to, and Re_{det} less than Re_{dl}. The threshold values for our classification scheme using the pressure criteria compare well with those using the incipient detachment criteria (figure 8). This means that geometries with $Re_{dl} < Re_{det}$ show inertial detachment; those with $Re_{dl} \approx Re_{det}$ show transitional detachment and those with $Re_{dl} > Re_{det}$ show creeping-flow detachment. An example for the case $Re_{dl} < Re_{det}$ was also reported by Lahbabi & Chang (1986), who showed numerically that $Re_{dl} \approx 5$, but $Re_{det} \approx 51$ for the geometry used in the experiments of Deiber & Schowalter (1979). A comparison between kinematics and dynamics is given in figure 11 for the case $Re_{dl} < Re_{det}$.

If then, there is generally no correspondence between the beginning of nonlinearity in the pressure–velocity relation and the onset of flow detachment, is there any relationship between the kinematic and the dynamic changes?

As already stated in § 3.1 for the curves with creeping flow detachment three regions can be distinguished (see figure 6): a first region in the low Re range, where the

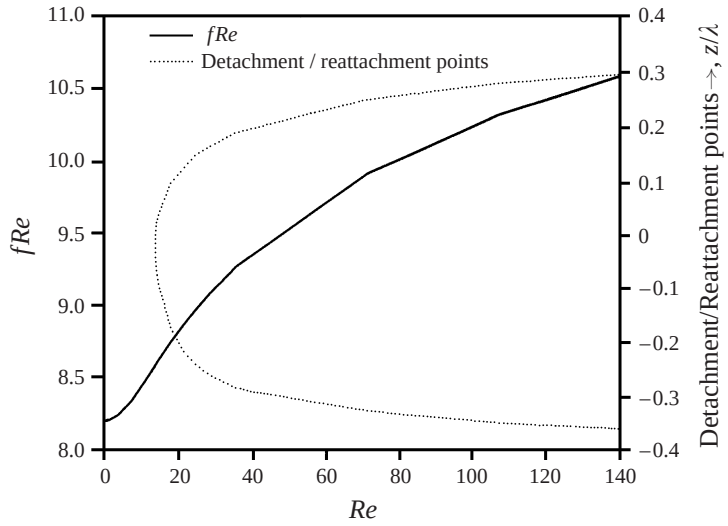

FIGURE 11. Comparison between 'relinearization' of the fRe curve and the widening of the detachment zones with $\delta = 0.35$ and $\gamma = 0.15$.

detachment zone remains constant in size independent of Re up to some limit named Re_{kl}; a second region, where the detachment zones grow more than logarithmically; and, after an inflection point, a third region, where they grow less than logarithmically with Re. For the geometries where incipient detachment occurs in the transitional range only the second and third regions can be found in figures 6 and 7. For the geometries where incipient detachment lies in the inertial range only the third region can be identified. From these facts we concluded above that creeping-flow detachment is correlated with zero growth of the detachment zone, transitional detachment with more than logarithmic growth and inertial detachment with less than logarithmic growth. A second fact can be added to support this conclusion. From table 3 one sees that the Reynolds numbers at which creeping-flow detachment zones start to expand and the beginning of the nonlinearity of the pressure drops observed for these geometries coincide, i.e. that $Re_{kl} \approx Re_{dl}$.

4.3. *Relinearization and the transition to turbulence*

Another question is how the gradual 'relinearization' at higher Re can be interpreted. Ralph (1987) found experimentally and numerically such a relinearized pressure–velocity relationship for $25 \leqslant Re \leqslant 300$ and transition to turbulence for larger Re. In fact Lahbabi & Chang's (1986) numerical solution for a different flow geometry predicted complete relinearization for $Re \geqslant 1000$, but for this geometry, the situation does not seem to occur experimentally: Deiber & Schowalter (1979) showed that the flow through the identical geometry becomes turbulent at $Re \approx 400$. Although our Re did not exceed 100 we found the beginning of relinearization for all flow geometries which we investigated. As can be seen in figure 11 the gradual flattening of the fRe-curve and the widening of the detachment zones occur simultaneously. A possible interpretation might be that the expansion of the detachment zones acts as if the wavy wall was being 'filled up' to take on the character of a straight tube both dynamically as well as kinematically. There is a fifth regime at high Re where the flow becomes turbulent. Although we know of no studies giving kinematic details for tubes, for channels Nishimura *et al.* (1983) found that the regions attain a maximum

Category → Aspect ↓	Creeping	Transitional	Inertial	Relinearized	Turbulent (after Nishimura *et al.*)
Symmetry	Symmetric	Symmetric	Asymmetric	Tending to symmetry	Oscillating, but symmetric in mean
Extent of detachment zone	Largest for large δ	Gradual inversion	Largest for small δ	Tending to equal size	?
Growth of detachment zone with Re	Constant size	More than logarithmic	Less than logarithmic	Tending to constant size	Reduced, at yet higher *Re* increased
Relation between kinematics and dynamics	$Re_{det} < Re_{dl}$	$Re_{det} \approx Re_{dl}$	$Re_{det} > Re_{dl}$	—	—

TABLE 4. Flow classification summary as *Re* increases.

z-extent of 78% for $Re = 400$, reducing to 69% at $Re = 5000$, after which they gradually increase again.

4.4. *Flow classification*

We have seen that there are a number of criteria according to which the flow discussed here can be classified. The most fundamental division is according to whether the flow is attached or not. When detached its form may be symmetric or asymmetric, where the boundary between the two only roughly corresponds to that between inertial and transitional flow (see relevant discussion in §3.18). All conclusions about flow classifications discussed above are summarized in table 4.

Two objections to this classification come to mind. First, the experimental and numerical data, although in good agreement, are too limited to make any claim to generality. The only way to see whether the scheme is sound, is to test it in further studies. Unfortunately Chow & Soda's (1972) attempt at a perturbation solution seems not be clear of error (see Hemmat & Borhan 1995 and Leneweit 1995), so that this task remains to be done. Secondly, the definitions of the limiting values Re_{dl} and Re_{kl} (the latter determined with the naked eye from figure 6) are too arbitrary to enable a really precise comparison between kinematics and dynamics. However, this criticism also applies to such concepts as, for example, that of boundary layer thickness. It thus remains to be seen whether the distinctions summarized in table 4 prove fruitful or not.

5. The effect of elongational strain rate in the flow through periodically constricted tubes and porous media

In the introduction we discussed work done on porous media, emphasizing the breakdown of the Darcy–Kozeny law as well as the discrepancy between estimations and empirically found values for the constant in the classical f–Re relationship for creeping flow. According to Bird *et al.* (1960, p. 129) the friction factor f_b of a porous medium can be derived from the tube friction factor f as given in (2.2) when the minimum tube radius R_{min} is replaced by twice the hydraulic radius R_h. This radius

is simply the ratio of the volume of the void space to the wettable surfaces of the porous medium. By idealizing the porous medium as a packed bed of spheres of equal diameter D_p one obtains

$$f_b = \frac{\Delta p}{\rho u_b^2} \frac{D_p}{L} \frac{\varepsilon^3}{(1-\varepsilon)}, \tag{5.1}$$

where u_b denotes the superficial velocity, L the length of the porous medium in the direction of flow and ε the ratio of the void volume to the total particle volume. When the pressure drop Δp is given by the Hagen–Poiseuille law using the hydraulic radius concept embodied in (5.1) one obtains

$$f_b = 72 \frac{(1-\varepsilon)\mu}{\rho D_p u_b} = \frac{72}{Re_b} \tag{5.2}$$

with the definition of the bed Reynolds number Re_b given implicitly. Equation (5.2) is usually referred to as the Darcy–Kozeny law. By evaluating the empirical data from several investigators Ergun (1952) found

$$f_b\, Re_b = 150 + 1.75 Re_b = \alpha_b + \beta_b\, Re_b, \tag{5.3}$$

where the influence of the nonlinear terms becomes noticeable for $Re_b = O(1)$. For periodically constricted tubes we found similar results to (5.3) for the pressure drops (see figure 10). The relationship between f and Re is well approximated for a large Re-range by the second-order polynomial $fRe = \alpha + \beta Re + \zeta Re^2$. For smaller $Re (Re < 90)$ before relinearization becomes apparent, the first two terms

$$fRe = \alpha + \beta Re \tag{5.4}$$

are adequate. In this Re-range, it is thus possible to compare the dynamic behaviour of porous media and periodically constricted tubes when the minimum tube radius R_{min} used in (2.2) is replaced by twice the hydraulic radius $2R_h$ in the definitions of Re (2.1) and f (2.2). Re and f are multiplied with a factor (3/2) and 3 respectively to yield Re_b and f_b. Then, (5.4) can be written as

$$f_b Re_b = \alpha_b + \beta_b Re_b. \tag{5.5}$$

Table 5 shows a comparison of the coefficients α_b and β_b of the periodically constricted tube and the porous medium. The values in table 5 show that for the tube geometries considered here the use of a tube with $\delta = 0.17$ and $\gamma = 0.15$ has the closest similarity to the dynamic behaviour of flows through porous media in the low Re-range ($Re < 90$). For higher Re dynamic similarities vanish because relinearization does not seem to occur in porous media flow. Now it was not our aim to optimize the dynamic agreement between tube flow and porous media flow, for which purpose one could certainly find geometries (in terms of the parameters γ and δ) that match better with the empirical data of porous media in the low Re-range. We, rather, ask the question whether the dynamically similar behaviour between porous media and tubes in the low Re-range reflected in table 5 gives any new insight into the behaviour of porous media. Is this the case?

Broaching the problem of the linear velocity term first, Durst *et al.* (1987) raised the question as to how the discrepancy between the theoretical and experimental values of α_b (72 and 150 or 182 respectively) can be explained. Now it is obvious that the introduction of the hydraulic radius concept and the neglect of the tortousity of the pores by replacing their length with the length of the porous medium in the direction of flow is a very simplified treatment where no exact agreement can be expected. Durst

γ	δ	α_b	β_b
0.21	0.11	738.68	10.23
0.21	0.29	96.48	1.41
0.21	0.79	32.88	0.03
0.15	0.17	205.74	1.44
0.15	0.35	78.75	0.30
0.15	0.85	45.18	0.06
porous medium (Ergun 1952)		150	1.75
porous medium (Durst *et al.* 1987)		182	1.75

TABLE 5. Comparison of α_b and β_b from (5.5) for periodically constricted tubes and a porous medium.

et al. showed that the pressure drop in an arbitrarily shaped tube is proportional to the energy dissipation $\Delta\dot{e}_{diss}$ per unit time in the flow volume considered, provided the surface integral over the inertial terms disappears. This holds for a periodically constricted tube with a laminar flow if $L = n\lambda (n = 1, 2, 3 \ldots)$:

$$\frac{\Delta p}{L} = \frac{1}{Q}\frac{(\Delta\dot{e}_{diss})}{L}.$$

They then suggested that the neglected elongational strain terms in the energy dissipation

$$\Delta\dot{e}_{diss} = \int_V \left\{ \underbrace{2\mu\left[\left(\frac{\partial u_r}{\partial r}\right)^2 + \left(\frac{u_r}{r}\right)^2 + \left(\frac{\partial u_z}{\partial z}\right)^2\right]}_{\text{elongational terms}} + \underbrace{\mu\left[\left(\frac{\partial u_r}{\partial z} + \frac{\partial u_z}{\partial r}\right)^2\right]}_{\text{shear terms}} \right\} \mathrm{d}V \qquad (5.6)$$

for an axisymmetric geometry without swirl would lead to an improvement in the theoretical estimate since only the underlined shear strain term in the energy dissipation is considered in the straight tube approximation made implicitly with the hydraulic radius concept. Unlike the flow geometry of a randomly packed bed of spheres investigated by Durst *et al.* (1987), our flow geometry admits an easy estimation of the energy dissipation in the Stokes limit $Re \to 0$, making use of the perturbational analysis by Chow & Soda (1972). To examine the above assumption, we need only to know the ratio of elongational to shear strain Θ:

$$\Theta = \frac{\displaystyle\int_V \left\{2\mu\left[\left(\frac{\partial u_r}{\partial r}\right)^2 + \left(\frac{u_r}{r}\right)^2 + \left(\frac{\partial u_z}{\partial z}\right)^2\right]\right\}\mathrm{d}V}{\displaystyle\int_V \mu\left(\frac{\partial u_r}{\partial z} + \frac{\partial u_z}{\partial r}\right)^2 \mathrm{d}V}. \qquad (5.7)$$

Table 5 showed that the geometry with $\delta = 0.17$ and $\gamma = 0.15$ gives a rough approximation of the dynamics in porous media. Since the geometry with $\delta = 0.11$ and $\gamma = 0.21$ gives an upper limit for both α_b and β_b we calculated Θ using (5.7) and found $\Theta = 0.56593$ for $\delta = 0.17$ and $\gamma = 0.15$ and $\Theta = 0.57317$ for $\delta = 0.11$ and $\gamma = 0.21$. Thus the energy dissipated due to elongational strain becomes maximally 3/5 of that dissipated by shear in a porous medium at low Re. From this it seems that the error in the theoretical determination of α_b arises both from the geometrical

simplifications (hydraulic radius, pore length) as well as from neglecting elongational strain.

The existence of relatively strong elongational strain for low-Re flow through porous media might give a hint to the solution of a further problem concerning the quadratic, or more generally, the nonlinear velocity terms, which are usually identified with inertial effects that can be determined for Re as low as $O(1)$. For it is the elongational strain term and the radial velocity u_r in the axial component of the steady incompressible axisymmetric Navier–Stokes equation without swirl,

$$\underbrace{\underline{u_r}\frac{\partial u_z}{\partial r} + u_z\frac{\underline{\partial u_z}}{\underline{\partial z}}}_{\text{convective inertial terms}} = -\frac{1}{\rho}\frac{\partial p}{\partial z} + \underbrace{\nu\Delta u_z}_{\text{viscous terms}}$$

(the underlined terms) which cause the convective inertial terms not to vanish as they do in straight laminar tube flow. Thus, inertia may well become apparent at much lower Re without the necessity for a transition to turbulent flow.

6. Conclusion

We have seen how the manner of increase of the detachment region with increasing Re (curvature, inflection points) is sensitive to geometrical parameters. Incipient detachment does not generally begin in a trough, but often upstream of it. For $\gamma \leqslant 0.15$ and $\delta \geqslant 0.94$ the detachment region showed no sign of decreasing, even down to $Re = 10^{-4}$. For a given γ the point of incipient detachment at Re_{det} moves upstream out of the trough as the tube narrows. We have also seen how the transition in the pressure drop from a linear Poiseuille-like behaviour to a nonlinear pressure drop–velocity relationship is not generally related the appearance of a detachment region, but rather to its form and the nature of its growth. We then looked at various possible criteria for determining the transition from the viscous to the inertial range. Finally, we discussed the effect of elongational terms in the energy dissipation for flow through periodically constricted tubes and compared this flow with the flow through porous media.

The question of the interplay between viscous and inertial forces is an interesting and still unanswered one. A study of the local pressure field might be helpful here, because, as mentioned at the outset, classical inertial detachment generally corresponds to the existence of an adverse pressure gradient. For example, does symmetric detachment have a significant effect on the local pressure field? A final question is whether a variational approach might be fruitful. The Stokes equations exhibit minimal dissipation: Stokes detachment zones thus dissipate less energy than any kinematically possible flow that obeys the same boundary conditions (theorem by Helmholtz, see e.g. Batchelor 1967). This property of Stokes flows might also give a hint to the understanding of the difference in the detachment conditions and their underlying mechanisms for asymmetric (inertial) and symmetric (transitional and creeping) detachment.

We thank Dr R. Kessler, DLR Göttingen, for supplying us with the numerical code and an unknown referee, for pointing out the effect of changing the reference radius from R_0 to R_{min} on some of the results.

REFERENCES

Andrade, J. S., Street, T., Shimohara, Y., Shibusa, Y. & Arai 1995 Percolation disorder in viscous and nonviscous flow through porous media. *Phys. Rev.* E **51**, 5725–5731.

Batchelor, G. K. 1967 *An Introduction to Fluid Dynamics*. Cambridge University Press.

Bird, R. B., Stewart, W. E. & Lightfoot, E. N. 1960 *Transport Phenomena*, p. 129. J. Wiley and Sons.

Chow, J. C. F. & Soda, K. 1972 Laminar flow in tubes with constriction. *Phys. Fluids* **15**, 1700–1706.

Collins, R. 1979 Separation from spherical caps in Stokes flow. *J. Fluid Mech.* **91**, 493–495.

Davis, A. M. J. & O'Neill, M. E. 1977 Separation in a slow linear shear flow past a cylinder and a plane. *J. Fluid Mech.* **81**, 551–564.

Davis, A. M. J., O'Neill, M. E., Dorrepaal J. M. & Ranger, K. B. 1976 Separation from the surface of two equal spheres in Stokes flow. *J. Fluid Mech.* **77**, 625–644.

Deiber, J. A., Peirotti, M. B., Bortolozzi, R. A. & Durelli, R. J. 1992 Flow of Newtonian fluids through sinusoidally constricted tubes. Numerical and experimental results. *Chem Engng Comm.* **117**, 241–262.

Deiber, J. A. & Schowalter, W. R. 1979 Flow through tubes with sinusoidal axial variations in diameter. *AIChE J.* **25**, 638–644.

Dorrepaal J. M. & O'Neill, M. E. 1979 The existence of free eddies in a streaming Stokes flow. *Qt J. Mech. Appl. Maths* **32**, 95–107.

Durst, F., Haas, R. & Interthal, W. 1987 The nature of flows through porous media. *J. Non-Newtonian Fluid Mech.* **22**, 169–189.

Ergun, S. 1952 Fluid flow through packed columns. *Chem. Engng Prog.* **48**, 89–94.

Fedkiw, P. & Newman, J. 1977 Mass transfer at high Péclet numbers for creeping flow in a packed bed reactor. *AIChE J.* **23**, 255–263.

Fedkiw, P. & Newman, J. 1987 Friction factors for creeping flow in sinusoidal periodically constricted tubes. *Chem Engng Sci.*, **42**, 2962–2963.

Firdaouss, M., Guermond, J.-L. & Le Quéré, P. 1997 Nonlinear corrections to Darcy's law at low Reynolds numbers. *J. Fluid Mech.* **343**, 331–350.

Forchheimer, P. 1901 Wasserbewegung durch Boden. *Z. Deutsche Ing.* **45**, 1736–1741; 1781–1788.

Guzman, A. M. & Amon, C. H. 1996 Dynamical flow characterization of transitional and chaotic regimes in converging-diverging channels. *J. Fluid Mech.* **321**, 25–57.

Hemmat, M. & Borhan, A. 1995 Creeping flow through sinusoidally constricted capillaries. *Phys. Fluids* **7**, 2111–2121.

Jeffrey, D. J. & Sherwood, J. D. 1980 Streamline patterns and eddies in low-Reynolds-number flow. *J. Fluid Mech.* **96**, 315–334.

Kececioglu, I. & Jiang, Y. 1994 Flow through porous media of packed spheres saturated with water. *Trans. ASME J. Fluids Engng* **116**, 164–170.

Lahbabi, A. & Chang, H.-C. 1986 Flow in periodically constricted tubes: transition to inertial and non-steady flows. *Chem. Engng Sci.* **41**, 2487–2505.

Leneweit, G. 1995 Ablösungs- and Widerstandsphänomene in periodisch-verengten Rohren bei niederen Reynolds-Zahlen Diplom-thesis. MPI f. Strömungsforschung, Bericht 5/1995.

Moffatt, H. K. 1964 Viscous and resistive eddies near a sharp corner. *J. Fluid Mech.* **18**, 1–18.

Munson, B. R., Rangwalla, A. A. & Mann, J. A. 1985 Low Reynolds number circular Couette flow past a wavy wall. *Phys. Fluids* **28**, 2679–2686.

Neira, M. & Payatakes, A. C. 1979 Collocation solution of creeping Newtonian flow through sinusoidal tubes. *AIChE J.* **25**, 725.

Nishimura, T., Yoshiji, O. & Kawamura. Y. 1983 Flow characteristics in a channel with symmetric wavy wall for steady flow. *J. Chem. Engng Japan* **17**, 466–471.

Patankar, S. V. & Spalding, D. B. 1972 A calculation procedure for heat, mass and momentum transfer in three-dimemsional parabolic flows. *Intl J. Heat Mass Transfer* **15**, 1787–1806.

Perić, M. 1985 A finite volume method for the prediction of three-dimensional fluid flow in complex ducts. PhD dissertation, University of London.

Perić, M., Kessler, R. & Scheuerer, G. 1988 Comparison of finite-volume numerical methods with staggered and colocated grids. *Computers Fluids* **16**, 389–403.

Petersen, E. E. 1954 Diffusion in a pore of varying cross section *AIChE J.* **4**, 343–345.

Pilitsis, S. & Beris, A. N. 1991 Viscoelastic flow in an undulating tube. Part II. Effects of high elasticity, large amplitude of undulation and inertia. *J. Non-Newtonian Fluid Mech.* **39**, 375–405.

Ralph, M. E. 1987 Steady flow structures and pressure drops in wavy-walled tubes. *Trans. ASME J. Fluids Engng* **109**, 255–261.

Rasoloarijaona, M. & Auriault, J.-L. 1994 Non-linear seepage flow through a rigid porous medium. *Eur. J. Mech.* B/*Fluids* **13**, 177–195.

Sobey, I. J. 1980 On flow through furrowed channels. Part 1. Calculated flow patterns. *J. Fluid Mech.* **96**, 1–26.

Stephanoff, K. D., Sobey, I. J. & Bellhouse, B. J. 1980 On flow through furrowed channels. Part 2. Observed flow patterns. *J. Fluid Mech.* **96**, 27–32.

Stone, H. L. 1968 Iterative solution of implicit approximations of multidimensional partial differential equations. *SIAM J. Numer. Anal.* **5**, 530–558.

Taneda, S. 1979 Visualization of separating Stokes flows. *J. Phys. Soc. Japan* **46**, 1935–1942.

Tilton, J. N. & Payatakes, A. C. 1984 Collocation solution of creeping Newtonian flow through sinusoidal tubes: a correction. *AIChE J.* **30**, 1016–1021.